Differential Acoustic Resonance Spectroscopy for the acoustic measurement of small and irregular samples in the low frequency range

Shang-xu Wang,[1] Jian-guo Zhao,[1] Zhen-hua Li,[1] Jerry M. Harris,[2] and Youli Quan[2]

Received 24 August 2011; revised 20 April 2012; accepted 23 April 2012; published 8 June 2012.

[1] Differential Acoustic Resonance Spectroscopy (DARS) has been developed to investigate the acoustic properties of samples in the kilohertz frequency range. This new laboratory measurement technique examines the change in resonant frequencies of a cavity perturbed by the introduction of a small test sample. The resonant frequency shift between the empty and sample-loaded cavity is used to estimate the acoustic properties of the loaded sample. This paper presents a DARS perturbation formula that combines a theoretical derivation with numerical simulation and laboratory measurements. Furthermore, a semi-empirical calibration technique is proposed to estimate the acoustic properties of a test sample. This research demonstrates the potential of the DARS measurement technique for estimating the acoustic properties of acoustically small and/or irregularly shaped samples.

Citation: Wang, S., J. Zhao, Z. Li, J. M. Harris, and Y. Quan (2012), Differential Acoustic Resonance Spectroscopy for the acoustic measurement of small and irregular samples in the low frequency range, *J. Geophys. Res.*, *117*, B06203, doi:10.1029/2011JB008808.

1. Introduction

[2] Several principal experimental methods exist to measure the acoustic properties as a function of frequency for samples ranging in compressibility from high (elastomers) to low (porous rock). Two common laboratory techniques that measure the acoustic properties of samples are pulse transmission and resonant bar methods [*Harris et al.*, 2005]. In pulse transmission, matched piezoelectric transducers are placed at the ends of the sample and used as a source and a receiver; this is also referred to as "pitch and catch." The ultrasonic pulse generated by the source is the "pitch," which travels through the sample and is the "caught" at the other end by the receiver. The wave propagation velocity can be calculated from the measured travel time of the pulse through a sample and the sample length. The attenuation can be derived by comparing waveforms that have traveled through the test sample with those that have traveled through a standard sample. Two types of transducers are used to generate pulses of compressional or shear waves, which are used to determine the compression and shear moduli, respectively. The pulse transmission technique operates in the hundreds of kilohertz range [*Birch*, 1960, 1961; *Wyllie et al.*, 1956; *Batzle et al.*, 2006].

[3] The resonant bar technique differs from pulse transmission in that it can operate in the kilohertz range. In this method, a cylindrical or parallelepiped sample is driven into or through a resonant vibration using a sinusoidal force. The numerous modes that are possible include length deformation, sensitive to the Young's modulus, and flexural and torsional deformations, sensitive to the shear modulus. These moduli are calculated from the resonant frequencies, the density, and the dimensions of the sample [*Adams and Coppendale*, 1976; *Lucet et al.*, 1991]. Previous researchers [*Winkler*, 1979; *Winkler et al*, 1979; *Clark*, 1980; *Tittmann et al.*, 1980; *Murphy*, 1982; *Bulau et al.*, 1983] used the resonant bar method to collect some of the first (and most importantly) low frequency data. *Yin et al.* [1992] and *Cadoret et al.* [1995] collected data in the kilohertz range and characterized the acoustic properties of sandstone and limestone samples. *Demarest* [1971], *Ulrich et al.* [2002], and *Zadler et al.* [2004] presented an extension of this method, resonant ultrasound spectroscopy (RUS), which uses a wide frequency range to capture numerous resonance peaks. RUS permits the determination of a suite of elastic constants by identifying the modes excited in a rock [*Migliori and Sarrao*, 1997; *Zadler et al.*, 2004]. However, as lower frequencies occur when using larger samples, the samples must be sufficiently durable and homogeneous such that long and narrow bars can be machined. Thus, sample preparation is extremely time consuming and often impractical.

[4] Stress-strain, a quasi-static method, is another important low-frequency measurement technique for determining

[1]CNPC Key Laboratory of Geophysical Prospecting, State Key Laboratory of Petroleum Resources and Prospecting, China University of Petroleum-Beijing, Beijing, China.
[2]Department of Geophysics, Stanford University, Stanford, California, USA.

Corresponding author: J. Zhao, CNPC Key Laboratory of Geophysical Prospecting, State Key Laboratory of Petroleum Resources and Prospecting, China University of Petroleum-Beijing, Changping District, Beijing 102200, China. (jgzhao761215@yahoo.com.cn)

the acoustic properties of samples. Stress-strain measurements, which record the forced deformation exerted on rock samples, have been performed for nearly a century to determine macroscopic mechanical properties. In these measurements, cyclic loading is used to subject a sample to deformations that are slow compared to the sample's natural mechanical resonances; thus, the sample is close to mechanical equilibrium at all times during the test. The sample's elastic moduli can be inferred from measurements of both the applied stresses as well as the induced strains. Despite some progress, the stress-strain technique is limited by the lack of advanced transducers, without which it is difficult to monitor extremely sensitive deformation. *Spencer* [1981] first applied this technique to rock samples, but the results were contaminated by boundary flow effects. Since that time, many researchers have worked in the field of forced oscillation. *Gribb and Cooper* [1998] designed a torsion apparatus, originally used for dynamic and static mechanical analyses of engineering materials, to investigate the seismic frequency and dynamic response of Earth's upper mantle. *Jackson et al.* [2011] developed laboratory equipment according to the forced oscillation method, which allows both torsional and flexural oscillation measurements at sub-micro strain amplitudes. The equipment provides seismic-frequency constraints on both the shear and compressional wave properties of cylindrical rock specimens. *Batzle et al.* [2006] developed a forced deformation system based on the stress-strain approach, which precisely monitors axial deformation using resistive strain gauges bonded directly to a test sample as transducers. As a result, this low frequency forced deformation system, in conjunction with a built-in pulse transmission assembly, can cover a very broad frequency band, from about 5 Hz to 800 kHz. Many laboratory measurements using this system have been taken for a variety of rock samples – shales, siltstones, tight sandstones, and carbonates – to investigate their acoustic properties. However, there are still some major challenges in applying this system: (1) extremely weak signals must be processed; (2) strain gauges are sensitive to the surface preparation of samples; and consequently, (3) the preparation of samples is time consuming. In addition, it is important to point out that test samples, in the aforementioned laboratory measurement techniques, must have a relatively large size and a regular shape. For pulse transmission measurements, the typical diameter and length of a cylindrical test sample are 2.5 cm and 5 cm, respectively. For the stress-strain technique, the typical sample size is about 3.8 cm in diameter and 5 cm in length. Samples for the resonant bar measurements need to be durable.

[5] This paper presents an alternative technique, the Differential Acoustic Resonance Spectroscopy (DARS) concept, to investigate the acoustic properties of a variety of samples in the one kilohertz frequency range. The DARS concept is based on perturbation theory. The resonant frequency of a fluid-filled cavity is dependent on the speed of sound in the fluid. The introduction of a sample (e.g., rock) perturbs the resonance properties of the cavity. The resonant frequency difference between the empty cavity (f_1) and the sample-loaded cavity (f_2) is used to predict the acoustic properties of the loaded sample. Figure 1 (top) shows the typical DARS response with and without a sample. The quality factor of the cavity is the resonant frequency f divided by the half-power bandwidth W of the resonance curve (Figure 1, top), namely, $Q = f/W$. The resonant frequency and half-power bandwidth can be found using Lorentzian curve fitting [*Mehl*, 1978]. When a sample is introduced, the resonance frequency increases or decreases depending primarily on the velocity and density properties of the sample and the sample's location in the cavity. A prototype of DARS was developed to demonstrate and test the underlying concept. The key component of the DARS apparatus is the cavity resonator, which can be spherical, rectangular, cylindrical, or any other shape. A cylindrical cavity resonator, immersed in a tank filled with silicone oil, was selected for the DARS prototype. A schematic diagram of this apparatus is shown in Figure 1 (bottom). A piezoceramic source shown in Figure 1 (bottom), placed at the bottom of the silicon oil tank, is used to excite the resonance. This source consists of a front cover of aluminum, a mechanic series system of ten piezoceramic discs, and a back cover of copper. The design is based on a few special considerations. In general, a single piezoceramic disc has good response characteristics in the high frequency range, and in this case, a mechanical series system of multiple-slice piezoceramics is utilized to provide good low frequency response without the need for high driven voltage. The density difference between the front and back covers enables good acoustic radiation directivity on the front. A high-sensitivity hydrophone (Reson TC4040) located at the top of the cavity is used to detect changes in the acoustic pressure signal. The hydrophone has a very wide frequency band, from 1 Hz to 120 KHz. A sample loaded in the cavity is moved vertically along the axis to test various pressure conditions. A computer-controlled stepper motor provides accurate and repeatable positioning of the sample. A lock-in amplifier is used to scan the frequency and to track and record a selected resonance curve. Using a step size of 0.1 Hz, a typical scan ranges from about 1035 Hz to 1135 Hz, which is around the natural resonance of the cavity. Using the DARS apparatus, *Xu et al.* [2006] and *Xu* [2007] successfully collected reliable data sets at about one kilohertz and estimated the compressibility of both nonporous and porous samples.

[6] A finite element simulation is implemented to better understand the DARS system and improve its accuracy in estimating the acoustic properties in a variety of test samples. As an application, we use DARS to measure the bulk modulus of a collection of rubber samples with irregular shapes. We demonstrate that the DARS apparatus, used in conjunction with a calibration approach, provides an alternative solution to the determination of the acoustic properties of small samples, as well as those with irregular shapes. This greatly increases the potential application of the DARS-based low frequency measurement technique, since earlier low frequency measurement techniques required large and regularly shaped samples.

2. Theoretical Framework

2.1. DARS Perturbation Theory

[7] The theoretical background employed in the DARS system, based on perturbation theory, is described in several SEG conference papers, technical reports, and a PhD thesis [*Harris et al.*, 2005; *Xu*, 2007; *Xu et al.*, 2006]. However,

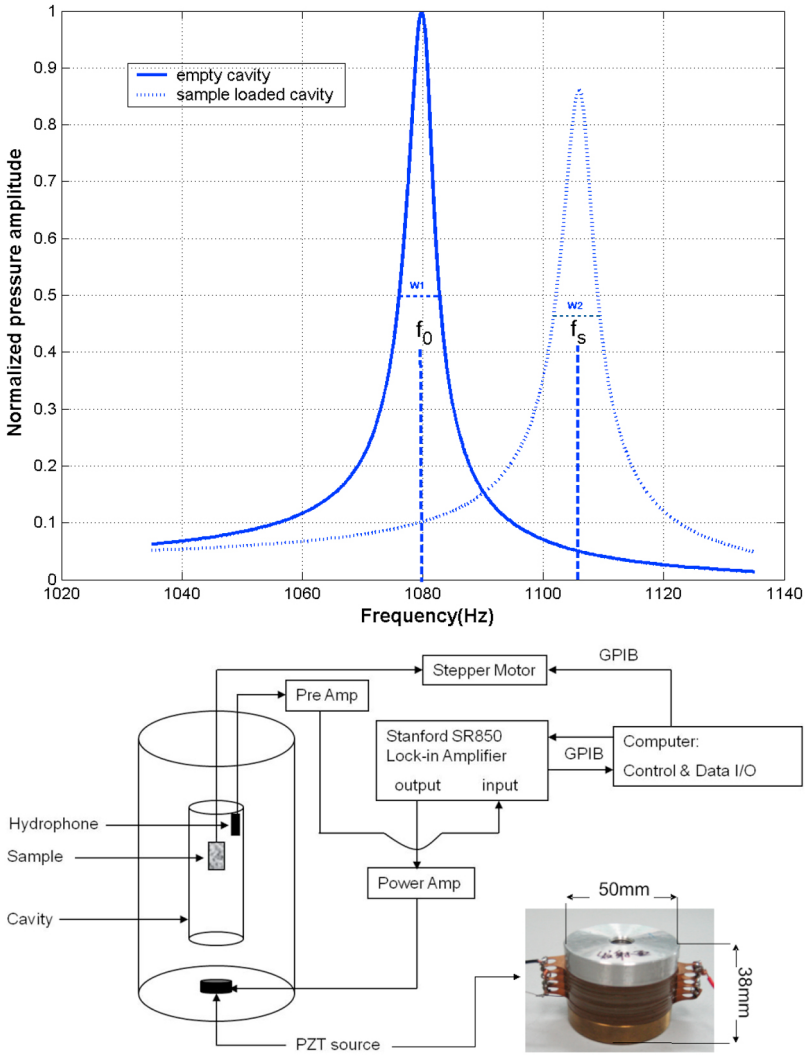

Figure 1. DARS setup and its response. (top) DARS responses with and without sample-loaded cavity. Two parameters, f_0 and f_s, are the resonant frequencies of the empty and sample-loaded cavity, respectively. (bottom) Diagram of the DARS setup. A cylindrical cavity with ends open is immersed in a tank filled with silicon oil. Source and receiver are connected to a lock-in amplifier through a power amplifier and a preamplifier, respectively. A computer-controlled stepper motor is used to control sample positioning.

since these relevant references are not readily available from a single source, the most important theoretical background is presented below.

[8] When resonance occurs in a fluid-filled cavity, as illustrated in Figure 1 (bottom), the standing wave inside the cavity produces a harmonic yet spatially varying pressure field along the longitudinal axis. The first longitudinal mode resonant frequency in the cylindrical cavity, equivalent to the first mode for the elementary problem of an organ pipe open at both ends, is well known:

$$f = \frac{c_0}{2L} \tag{1}$$

where c_0 is the sound speed of the fluid filling the cavity and L is the cavity length. Thus, the acoustic pressure has a sinusoidal distribution in the longitudinal direction. The particle velocity is proportional to the spatial derivative of the acoustic pressure. Accordingly, there are two particular locations, the acoustic pressure node and the particle velocity node, which correspond to the middle of the cavity and the two open ends of the cavity, respectively. For the fundamental mode, the acoustic pressure node is the location where the particle velocity is at its maximum. A velocity node occurs where the acoustic pressure is at its maximum.

[9] As illustrated in Figure 1 (bottom), the introduction of a test sample perturbs the resonance properties of the fluid-filled cavity. Suppose that p_1 and p_2 are the pressure distributions along the cavity axis, namely, $p_1(z)$ and $p_2(z)$, during resonance before and after the introduction of the test sample, respectively. Accordingly, the resonant angular frequency shifts from ω_1 to ω_2 due to the influence of the perturbation. The derivation below is adapted from microwave cavities [*Sucher and Fox*, 1963; *Chen et al.*, 1999] for application to acoustic cavities. Consider two slightly different cavities, distinguished by subscripts that correspond to

the sample-free and the sample-loaded cases. The frequency domain acoustic wave equations for these two cavities can be expressed as

$$-\kappa_1\omega_1^2 p_1 = \nabla\cdot\left(\frac{1}{\rho_1}\nabla p_1\right), \tag{2}$$

$$-\kappa_2\omega_2^2 p_2 = \nabla\cdot\left(\frac{1}{\rho_2}\nabla p_2\right). \tag{3}$$

Here, $\kappa_i = 1/(\rho_i c_i^2)(i = 1, 2)$ is the compressibility of the material with c_i and ρ_i the sound speed and density, respectively. In general, the angular frequencies ω_i are complex to reflect all losses. Assume that the cavity fluid has a constant compressibility κ_0 and the test sample has a constant compressibility κ_s. Then κ_1 equals κ_0 everywhere in the cavity, and κ_2 equals κ_s at the sample location and equals κ_0 otherwise.

[10] There are two types of boundary conditions for this resonance problem: $p_i = 0$ (soft boundary or free boundary condition) at the two open ends of the cavity, and $\nabla p_i \cdot \mathbf{n} = 0$ (hard boundary or rigidity boundary condition) on the inner and outer surfaces of the cavity, where $\mathbf{n}$ represents the normal direction of the cavity surface. The physical meaning of "soft boundary" is that the acoustic pressure is zero at the two open ends of the cavity, while the rigidity boundary means that the particle velocity equals zero in the direction perpendicular to the cavity surface. It should be noted that the material used for the cavity is not completely rigid, and thus the condition $\nabla p \cdot \mathbf{n} = 0$ is not strictly true. Therefore, the resonance frequency predicted by the eigen-frequency solution (see section 3 DARS simulation) may not be exactly equal to the real resonance frequency. However, because DARS uses the differential resonance frequency (obtained from standard and test samples) to estimate the properties of test samples, the effects of this error can be somehow canceled.

[11] Equations (2) and (3) can be solved with these boundary conditions. Multiplying (2) by p_2 and (3) by p_1, and integrating over the cavity volume (V_C), we have

$$-\int_{V_C}\kappa_1\omega_1^2 p_1 p_2 dV = \int_{V_C}\nabla\cdot\left(\frac{1}{\rho_1}\nabla p_1\right)p_2 dV, \tag{4}$$

$$-\int_{V_C}\kappa_2\omega_2^2 p_1 p_2 dV = \int_{V_C}\nabla\cdot\left(\frac{1}{\rho_2}\nabla p_2\right)p_1 dV. \tag{5}$$

Employing divergence (Gauss's) theorem, we can write $\int_{V_c}\nabla\cdot\left(\frac{1}{\rho_1}\nabla p_1\right)p_2 dV = \int_{S_c} p_2\frac{1}{\rho_1}(\nabla p_1\cdot\mathbf{n})dS - \int_{V_c}\frac{1}{\rho_1}\nabla p_1\nabla p_2 dS$, where the surface integral is taken over the cavity surface. The boundary conditions $p_i = 0$ and $\nabla p_i \cdot \mathbf{n} = 0$ lead to $\int_{S_c} p_2\frac{1}{\rho_1}(\nabla p_1\cdot\mathbf{n})dS = 0$. We then find

$$-\int_{V_C}\kappa_1\omega_1^2 p_1 p_2 dV = -\int_{V_C}\frac{1}{\rho_1}\nabla p_2\cdot\nabla p_1 dV, \tag{6}$$

$$-\int_{V_C}\kappa_2\omega_2^2 p_1 p_2 dV = -\int_{V_C}\frac{1}{\rho_2}\nabla p_1\cdot\nabla p_2 dV. \tag{7}$$

After subtracting equation (7) from equation (6) and with further manipulation, we finally obtain

$$\omega_2^2 - \omega_1^2 = -\omega_2^2\frac{\kappa_s-\kappa_0}{\kappa_0}\frac{V_S}{V_C}A - \omega_1^2\frac{\rho_s-\rho_0}{\rho_s}\frac{V_S}{V_C}B, \tag{8}$$

where

$$A = \frac{V_C}{V_S}\int_{V_S} p_1 p_2 dV \Big/ \int_{V_C} p_1 p_2 dV,$$

$$B = \frac{V_C}{V_S}\frac{1}{k_1^2}\int_{V_S}\nabla p_1\cdot\nabla p_2 dV \Big/ \int_{V_C} p_1 p_2 dV.$$

Here, $k_1 = \omega_1/c_1$ is the wave number and V_S is the volume of the test sample. Denote the coefficients A and B in equation (8) as $\langle p_1 p_2\rangle$ and $\langle\nabla p_1 \cdot \nabla p_2\rangle$, which are the average acoustic pressure and the particle velocity over the cavity volume. Here we use ω_0 and ω_s to denote the resonant frequencies of the cavity with and without the sample, and ρ_0 and ρ_s to denote the densities of the cavity fluid and test sample, respectively. Thus, equation (8) can be rewritten as

$$\omega_s^2 - \omega_0^2 = -\omega_s^2 V_S\frac{\kappa_s-\kappa_0}{\kappa_0}\langle p_1 p_2\rangle - \omega_0^2 V_S\frac{\rho_s-\rho_0}{\rho_s}\langle\nabla p_1\cdot\nabla p_2\rangle. \tag{9}$$

Equation (9) is the DARS perturbation equation.

2.2. Method to Determine Compressibility

[12] Two terms in equation (9), the compressibility contrast $(\kappa_s - \kappa_0)/\kappa_0$ and the density contrast $(\rho_s - \rho_0)/\rho_s$ between the test sample and cavity fluid, contribute to the frequency shift as shown in Figure 1 (top). In general, the density of a test sample is easy to measure. Thus, determining the compressibility of a test sample is a larger concern for the DARS measurements. If a test sample is measured at a velocity node (or acoustic pressure antinode) where $\langle\nabla p_1 \cdot \nabla p_2\rangle$ vanishes, the second term can be eliminated. As a result, equation (9) is simplified to

$$\omega_s^2 - \omega_0^2 = -\omega_s^2 V_S\frac{\kappa_s-\kappa_0}{\kappa_0}\langle p_1 p_2\rangle. \tag{10}$$

Ignoring second- or higher-order infinitesimals of $\Delta\omega = \omega_s - \omega_0$, applying the identity $(\omega_s^2 - \omega_0^2) = (\omega_s + \omega_0)(\omega_s - \omega_0)$, and assuming $p_2 \approx p_1$, we can rewrite equation (10) as

$$\frac{\omega_s-\omega_0}{\omega_0} = -CV_S\frac{\kappa_s-\kappa_0}{\kappa_0}, \tag{11}$$

where $C = -\frac{1}{2}\langle p_1^2\rangle$ is a calibration coefficient.

[13] The calibration coefficient C, a constant, is related to the geometry of the cavity and the experimental conditions such as the temperature and ambient pressure. Estimating the compressibility of a test sample requires obtaining a reasonable calibration coefficient through a standard sample, whose volume is expected to be close to that of the test sample as much as possible. Also, the simplified DARS perturbation equation (11) shows a linear relationship between the compressibility contrast $\delta\kappa = (\kappa_s - \kappa_0)/\kappa_0$ and the resonant frequency contrast $\delta f = (f_s - f_0)/f_0$. In the

Table 1. Sample Parameters and Resonant Frequencies at Certain Decimated Data Points

Sample	Sonic Velocity (m/s)	Density (kg/m^3)	Frequency (Hz)	k (Gpa^{-1})
1	960	960	1266.669	1.13028
2	980	1000	1271.572	1.04123
3	1000	1040	1275.998	0.96154
4	1040	1080	1281.925	0.85607
5	1080	1120	1287.064	0.76548
6	1200	1180	1297.258	0.58851
7	1400	1250	1307.83	0.40816
8	1600	1350	1314.879	0.28935
9	1800	1450	1319.451	0.21286
10	2000	1540	1322.484	0.16234
11	2400	1600	1325.746	0.10851
12	2800	1800	1327.996	0.07086
13	3000	1900	1328.731	0.05848
14	3500	2000	1329.794	0.04082
15	4000	2100	1330.453	0.02976
16	5000	2300	1331.176	0.01739
17	6000	2500	1331.528	0.01111
18	7000	2700	1331.715	0.00756

following section we describe a systematic simulation study, using the 18 numerical simulations shown in Table 1, to validate the linearity and further investigate the calibration of the DARS system.

3. DARS Simulation

3.1. Amending DARS Perturbation Formula

[14] In order to understand the validity limits of the DARS perturbation formula as shown in equation (11), we perform a comprehensive simulation study using the finite element method (using the commercial software COMSOL). As shown in Figure 1 (bottom), a key component of the DARS system is a cylindrical cavity with two open ends that is immersed in silicone oil. Figure 2a shows the DARS model used in the simulation. We use a two-dimensional rectangle to simulate the cavity, which allows us to obtain the highest numerical accuracy and explore the key physics features of the technique. In the DARS model, the sound speed and density of the cavity fluid are 960 m/s and 908 kg/m^3, respectively. A typical pressure distribution corresponding to the first-mode resonant frequency is plotted on the right of Figure 2a. Noticeably, the DARS simulation conducted in this work is to mathematically solve an eigen-frequency problem with the boundary conditions, $p = 0$ (free boundary) for the top and bottom (open) sides of cavity, and $\nabla p_i \cdot \mathbf{n} = 0$ (rigidity boundary) for the left and right sides of the cavity. For a test sample introduced to the cavity system, a continuity boundary condition is applied to the interface between the sample and its surrounding fluid. Such settings of boundary conditions enable the observation of resonance phenomena comparable to laboratory measurements. Contrarily, if we apply the continuity boundary conditions, instead of $\nabla p_i \cdot \mathbf{n} = 0$ (rigidity boundary), to the interfaces between the cavity wall and the fluid, no resonance occurs; if we apply a rigidity boundary to the surface of a test sample, the estimated compressibility from DARS is always zero. The two cases do not conform to the physical measurements of DARS.

[15] In the DARS simulations, for the empty cavity (in which the acoustic property of a test sample is the same as the surrounding fluid), the resonant frequency of the first mode is 1263.158 Hz. We then change the density and sound speed of the sample to investigate how the resonant frequency changes as the sample property changes. For simplicity, the test sample is only placed at the center of the cavity. In the laboratory experiment, however, a complete profile of resonant frequencies can be acquired as the sample moves along the longitudinal axis. Table 1 lists 18 synthetic samples with different acoustic properties. In the simulation these samples are used to obtain the first mode eigen-frequencies. These

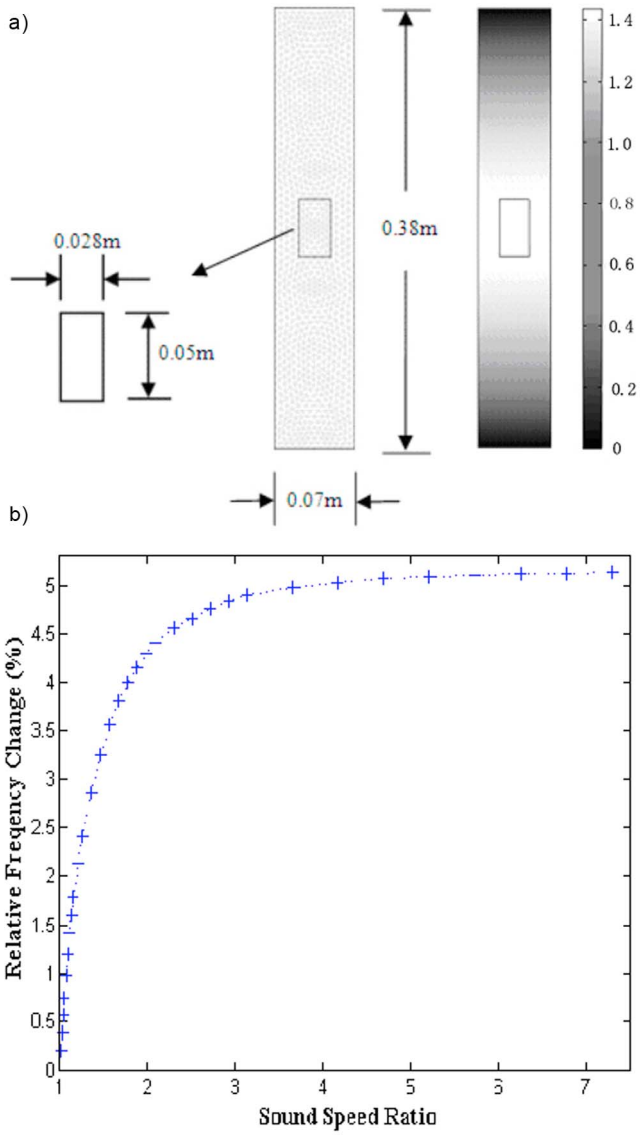

Figure 2. Two-dimensional DARS simulation. (a) The two-dimensional DARS model used in the finite element simulation. The sonic velocity of the cavity fluid is 960 m/s, and the density is 908 kg/m^3. A sample sized 0.028 × 0.05 m^2 is placed at the center of the rectangular cavity. The triangular mesh is also shown along with the cavity model. The pressure distribution corresponding to the first resonant frequency is shown on the right. (b) Normalized sonic velocity for the sample versus resonant frequency change for the cavity. The horizontal axis is the ratio of the sonic velocity of sample to that of surroundings.

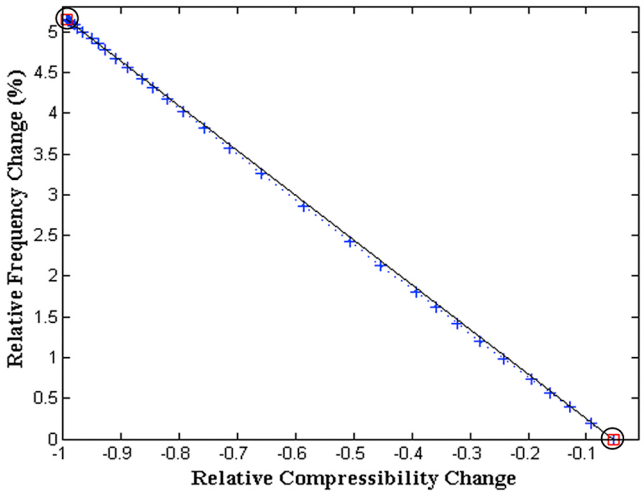

Figure 3. Normalized sample compressibility change versus normalized resonant frequency change. Plus signs show simulation results, and the solid line links the first and the last points indicated by the squares/circles. There is a small deviation between data points and the straight line.

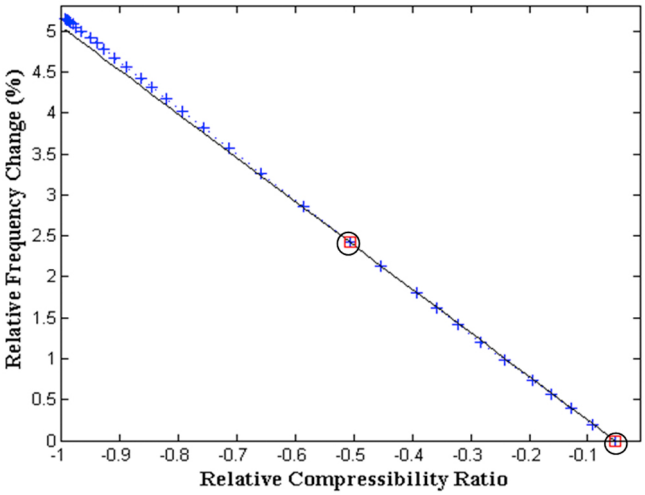

Figure 4. Calibration performed with a standard sample of medium compressibility. The solid straight line represents the perturbation formula corresponding to this calibration. The deviation between data points and the straight line is large for those samples with low compressibility.

eigen-frequencies and their compressibility, defined by $\kappa_i = (\rho_i c_i^2)^{-1}$, are also listed in Table 1. Figure 2b plots the resonant frequency contrast δf versus the ratio of the sample sound speed to the cavity fluid sound speed. This plot clearly indicates that the resonant frequency is more sensitive to the introduction of a test sample if it has a smaller acoustic contrast to the surrounding cavity fluid. With a less compressible test sample (one with a lower compressibility), the sensitivity becomes less pronounced. This indicates that the measurement of less compressible test samples may produce larger estimation errors and we need to pay special attention to the measurements in these cases.

[16] As a consequence, the simulation results shown in Table 1 have been employed to examine the linearity between the compressibility contrast $\delta\kappa$ and the resonant frequency contrast δf, as described in the following perturbation equation

$$\delta f = CV_S \delta\kappa. \tag{12}$$

This equation is just a different form of equation (11). Figure 3 is a scatterplot of $\delta\kappa$ versus δf. The solid straight line in this plot connects the first and last data points. It is observed that the sample compressibility contrast $\delta\kappa$ and the resonant frequency δf retain an approximate linear relationship over a large range. However, samples with low compressibility fall within a small range although they still exhibit a linear relationship. On the other hand, if we instead select a standard sample of medium compressibility (sample No. 10 in Table 1) to calculate the calibration coefficient (Figure 4), the estimation error of the compressibility of the less compressible samples, based on equation (12), becomes very large. Strictly speaking, both Figures 3 and 4 show that the relationship between $\delta\kappa$ and δf is not perfectly linear. This indicates that the calibration coefficient C in equation (12) is not strictly a constant. What causes the slight nonlinearity shown in Figures 3 and 4? A study of the derivation of the DARS perturbation equation indicates that the answer lies in the assumption that the acoustic pressure field remains uniform regardless of the type of sample introduced into the empty cavity. That is to say, the sample-induced pressure field p_1 is always equal to the pressure field p_0 of the empty cavity. Through the simulation, we can obtain three slightly different pressure field distributions, p_0, p_1, and p_2 (Figure 5), which correspond to three particular measurement scenarios, an empty cavity and two different standard sample-induced cavities, respectively. We can examine this effect when using

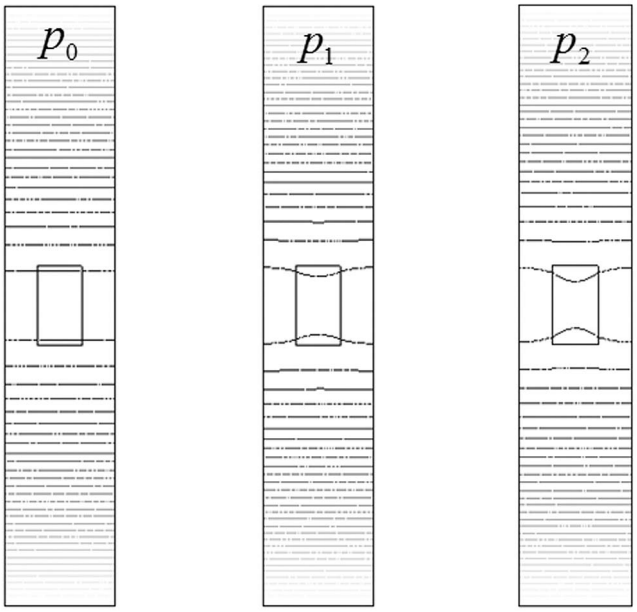

Figure 5. Pressure contours within the cavity for three different cases: (left) empty cavity, (middle) standard #1 sample-loaded cavity and (right) standard #2 sample-loaded cavity, respectively. Standards #1 and #2 are corresponding to samples 10 and 18 in Table 1. The introduction of a sample will slightly change the pressure distribution.

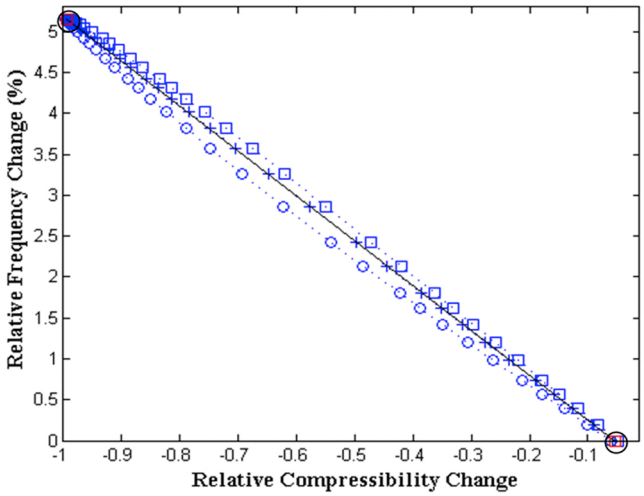

Figure 6. Scatterplots of δf versus $[(\kappa_s/\kappa_0)^b - 1]$ with $b = 1.1$ (circle), 0.9736 (+), and 0.9 (square), respectively.

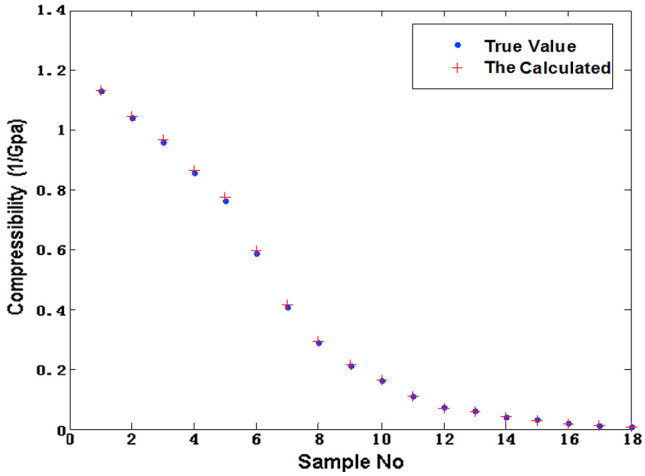

Figure 7. Comparison between the calculated compressibility parameters of the 18 samples listed in Table 1 and their true values. The calculation is based on the amended DARS perturbation formula, and samples No.10 and No.18 are used as two standard samples for calibration.

p_0 as an approximation to p_1 and p_2 for the calibration coefficient C. Let

$$\langle p_0 p_1 \rangle = \int_{V_s} p_0 p_1 dV.$$

Using the simulated pressure field shown in Figure 5, we find that the relative error $(\langle p_0 p_1 \rangle - \langle p_0 p_0 \rangle)/\langle p_0 p_0 \rangle = -1.6\%$, and $(\langle p_0 p_2 \rangle - \langle p_0 p_0 \rangle)/\langle p_0 p_0 \rangle = -1.7\%$. This sample-induced effect on the calibration coefficient C results in the nonlinearity revealed in Figures 3 and 4. If we can reduce the nonlinearity described above by making the data points in Figure 3 or Figure 4 better fit a straight line, the applicability of the DARS perturbation formula will be expanded into a larger compressibility range. Motivated by this observation, we conjecture that a proper model parameter can be used to improve the linearity of the relationships shown in Figures 3 and 4. The following semi-empirical perturbation equation is proposed:

$$\delta f = \left[(\kappa_s/\kappa_0)^b - 1\right] C$$

or

$$\kappa_s = [\delta f / C + 1]^{1/b} \kappa_0. \tag{13}$$

There are two calibration parameters C and b in equation (13); therefore, two standard samples are needed for their calculation. Along with simulation data, Figure 6 shows the tests on equation (13) for different b values. The curvature of the data points varies with b. A value of $b = 0.9736$ provides the best fit to the straight line over the entire compressibility range. When $b = 1$, equation (13) is reduced to equation (12); the scatterplot for this case is shown in Figure 3.

[17] To validate the effectiveness of the amended DARS perturbation formula described in equation (13), we apply it to the simulation data from the 18 synthetic samples listed in Table 1. We then compare the calculated compressibility with their true values. As shown in Figure 7, the amended formula produces a good estimation over the entire compressibility range. For completeness we also obtain results based on the calibration indicated in equation (12) for one standard sample. The estimation error is calculated in both cases and compared as listed in Table 2. The amended DARS perturbation formula has a noticeably improved estimation error compared to the original one over a large compressibility range. However, the original DARS perturbation formula should be capable of a more accurate estimation when measuring a relatively less compressible test sample with a standard sample of low compressibility, for instance, aluminum.

Table 2. Comparison of Compressibility Parameters Between True Values and Estimation Results Through Equations (12) and (13)[a]

		Estimation From Two Samples		Estimation From One Sample	
Sample	k (Gpa^{-1})	k_2 (Gpa^{-1})	Error	k_1 (Gpa^{-1})	Error
1	1.13028	1.13319	0.26%	1.13419	0.35%
2	1.04123	1.04696	0.55%	1.04927	0.77%
3	0.96154	0.96922	0.80%	0.97261	1.15%
4	0.85607	0.86529	1.07%	0.86995	1.62%
5	0.76548	0.77536	1.29%	0.78094	2.02%
6	0.58851	0.59751	1.53%	0.60437	2.70%
7	0.40816	0.41405	1.44%	0.42126	3.21%
8	0.28935	0.29248	1.08%	0.29916	3.39%
9	0.21286	0.21408	0.57%	0.21997	3.35%
10	0.16234	0.16234	0.00%	0.16745	3.15%
11	0.10851	0.10701	−1.38%	0.11094	2.25%
12	0.07086	0.06987	−1.40%	0.07197	1.57%
13	0.05848	0.05682	−2.82%	0.05924	1.31%
14	0.04082	0.03911	−4.16%	0.04083	0.04%
15	0.02976	0.02820	−5.22%	0.02941	−1.16%
16	0.01739	0.01632	−6.15%	0.01689	−2.86%
17	0.01111	0.01059	−4.73%	0.01079	−2.82%
18	0.00756	0.00756	0.00%	0.00756	0.00%

[a]A standard sample, No. 18 in Table 1, is used for calibration in equation (12), and two standard samples, No.18 and No.10 in Table 1, for the determination of calibration coefficient C and b in equation (13).

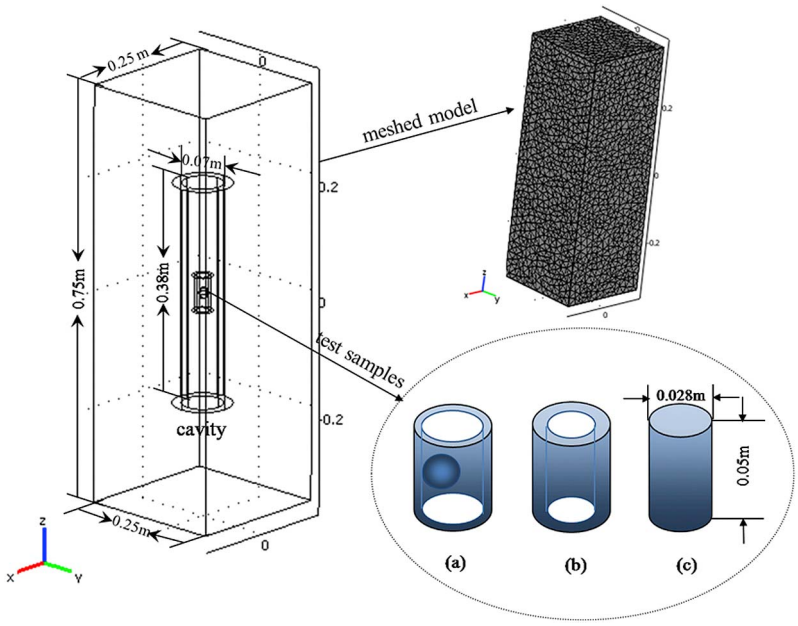

Figure 8. The three-dimensional DARS model used in the finite element simulation. The sonic velocity for the cavity fluid is 960 m/s, and the density is 908 kg/m^3. Three test samples, a cylindrical tube with a sphere attached inside (sample a), a cylindrical tube (sample b), and a solid cylinder (sample c), with the same volume are placed at the center of a cylinder cavity. The simulation is to confirm that the resonant measurements are independent of the shapes of test samples with the same volume and material. It provides the theoretical basis for DARS to deal with the determination of the acoustic properties of test samples with irregular shapes.

3.2. Applicability of DARS to Irregular Samples

[18] It is seen from the DARS perturbation formula, equation (8), that the resonant frequency shift is explicitly dependent on the volume of a test sample rather than its shape. Therefore, we suggest that the DARS technique is potentially applicable to the estimation of the acoustic properties of irregularly shaped samples, as long as the sample volume can be accurately quantified (in most cases this is not a big challenge). On the basis of the two-dimensional simulation, we implemented a three-dimensional DARS simulation to confirm this conclusion. Figure 8 illustrates the three-dimensional DARS simulation and the meshed model used in the finite element analysis. The properties of the cavity fluid remain the same as in the two-dimensional simulation. Also, the boundary conditions for the open-ended cavity are similar to those used in the two-dimensional simulation. However, the three-dimensional DARS model uses a rectangular silicon oil tank. In the simulation, the hard boundary condition is applied to the inner surfaces of the tank, while the soft boundary condition is used for the top surface, keeping in mind that DARS is an open system. We implemented the simulation for the 18 samples listed in Table 1. Each of these samples is assumed to have one of these three shape types: (a) a cylindrical tube with a sphere attached inside, (b) a cylindrical tube, or (c) a solid cylinder with the same volume. The simulated resonant frequencies for the 18 samples and three shape types are shown in Figure 9. The behavior validates that the resonant frequencies are independent of the shape of a test sample.

3.3. Dimension Limitations of the DARS Sample

[19] With the current DARS measurements, equation (10) or (11) is used to determine the compressibility of a test sample, while equation (8) or (9) presents a complete perturbation formula. This implies that a test sample must be measured at a velocity node or at an acoustic pressure antinode. Consequently, the sample needs to be small enough relative to the cavity so that the measurement is considered to be at a node. When a test sample is measured at a velocity node, equation (8) is reduced to the following form:

$$\omega_2^2 - \omega_1^2 = -\omega_2^2 \frac{\kappa_s - \kappa_0}{\kappa_0} \frac{V_S}{V_C} A.$$

Furthermore, the above equation is rewritten as

$$\delta f = \left(-A \frac{\kappa_s - \kappa_0}{\kappa_0} \right) \delta V \tag{14}$$

where $\delta f = (f_2^2 - f_1^2)/f_2^2$, $\delta V = V_S/V_C$. A, a calibration efficient in the DARS measurements, has a constant value independent of the test samples. Obviously, δf and δV should retain a strictly linear relationship for a test sample with a fixed κ_s of the compressibility.

[20] A numerical study is conducted to investigate how volume changes in a test sample relative to the cavity affect the accuracy of the DARS measurements. This is done by assessing the linearity in equation (14). The three-dimensional DARS model (Figure 8) is used for the simulation. All settings including the boundary conditions and the properties of the

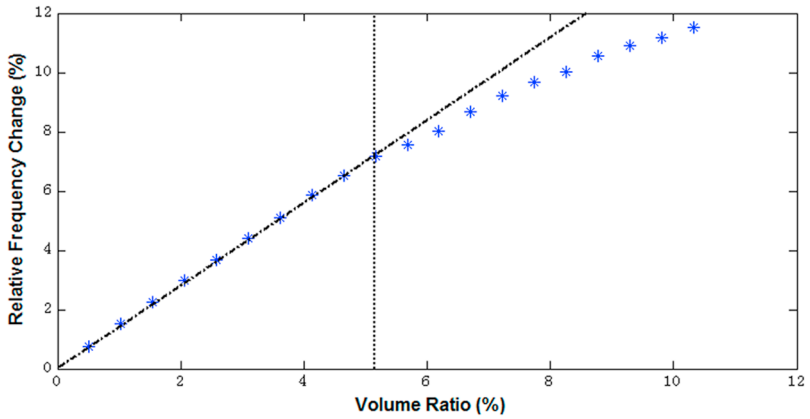

Figure 9. Investigation on the linearity between the resonance frequency contrast, $(f_2^2 - f_1^2)/f_2^2$, and the relative volume, Vs/Vc based on the three-dimensional DARS simulations. A DARS measurement model shown in Figure 8 is used, and all settings including boundary and the properties of cavity fluid remain exactly the same (see Table 3).

cavity fluid remain exactly the same. A synthetic cylinder sample, with a sonic velocity and density of 2000 m/s and 1540 kg/m^3, respectively, is used in the DARS measurement model. The diameter of the synthetic cylinder sample is constant at 3.1 cm, and its length increases from 1 cm to 19 cm in the numerical experiment. Table 3 lists the details of the simulation, and Figure 10 shows a scatterplot of $\delta f = (f_2^2 - f_1^2)/f_2^2$ versus $\delta V = V_S/V_C$. It is observed that the resonance frequency contrast δf and the volume ratio δV display almost perfect linearity when δV is less than 5%, otherwise the linearity is lost. This observation indicates that a test sample can be considered "small enough" to be measured at a velocity node, and justifies the use of the perturbation equation (10) when the sample volume relative to the DARS cavity is less than 5%. However, a relative volume over 5% results in a poor estimate from perturbation theory.

[21] While the aforementioned comments on the limitations of a sample volume are inferred from a regularly shaped sample, they also provide some insight into irregular samples. The "irregularity" of a sample cannot be arbitrarily determined; however, the relative volume should be less than 5%. This means that the surface distribution of an irregular sample needs to be concentrated at its centroid as much as possible. At the extreme is a sample which has an infinitesimal thickness in the axial direction, but has a longitudinal distribution from the cavity top to its end. In this case, the sample is assuredly small relative to the resonant tubing in terms of its volume; however, it is too large in the longitudinal direction to be considered to be measured at a velocity node with a view of pressure distribution inside the

Table 3. Three-Dimensional DARS Simulations on the Effect of the Relative Volume, Vs/Vc, Between a Test Sample and Cavity on the Resonance Frequency Contrast, $(f_2^2 - f_1^2)/f_2^2$[a]

Sample	Diameter (m)	Length (m)	V_S (10^{-6}·m^3)	f_2 (Hz)	V_S/V_c (%)	$(f_2^2-f_1^2)/f_2^2$ (%)
1	0.031	0.01	7.547676	1155.34	0.5161	0.7464
2	0.031	0.02	15.09535	1159.76	1.0322	1.5015
3	0.031	0.03	22.64303	1164.19	1.5483	2.2497
4	0.031	0.04	30.19070	1168.47	2.0644	2.9645
5	0.031	0.05	37.73838	1172.86	2.5806	3.6896
6	0.031	0.06	45.28606	1177.33	3.0967	4.4195
7	0.031	0.07	52.83373	1181.59	3.6128	5.1074
8	0.031	0.08	60.38141	1185.02	4.1289	5.6560
9	0.031	0.09	67.92909	1189.75	4.6450	6.4046
10	0.031	0.10	75.47676	1193.68	5.1611	7.0199
11	0.031	0.11	83.02444	1197.26	5.6772	7.5751
12	0.031	0.12	90.57211	1200.13	6.1933	8.0167
13	0.031	0.13	98.11979	1204.54	6.7095	8.6890
14	0.031	0.14	105.6675	1208.12	7.2256	9.2293
15	0.031	0.15	113.2151	1211.15	7.7417	9.6829
16	0.031	0.16	120.7628	1213.52	8.2578	10.0354
17	0.031	0.17	128.3105	1216.93	8.7739	10.5388
18	0.031	0.18	135.8582	1219.39	9.2900	10.8994
19	0.031	0.19	143.4058	1221.38	9.8061	11.1895
20	0.031	0.20	150.9535	1223.56	10.3222	11.5057

[a]In the simulation, the resonance frequency and volume of cavity are f_1 = 1151.02 Hz, and, Vc = 1462.411(10^{-6}·m^3), and a synthetic cylinder sample, whose sonic velocity and density are 2000 m/s and 1540 kg/m^3, respectively, are utilized in the DARS measurements simulation.

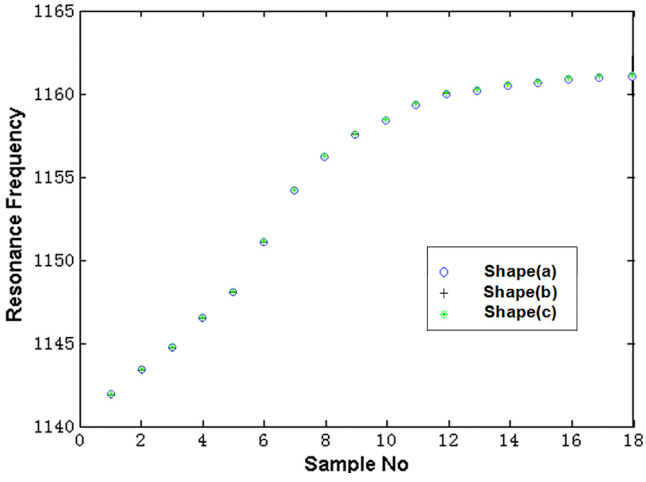

Figure 10. Comparison between the three-dimensional DARS simulation based resonant frequencies for 18 test samples with three different shapes shown in Figure 8. The parameters of density and sound speed for the 18 samples are listed in Table 1.

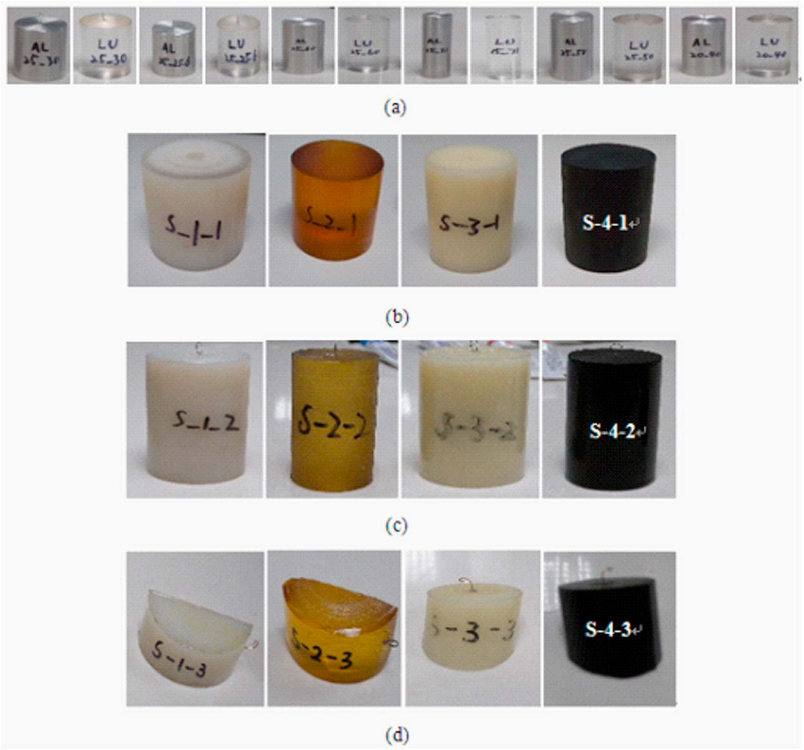

Figure 11. Samples for DARS and ultrasonic pulse transmission measurements. (a) Six pairs of standard Aluminum and Lucite samples, (b) Group #1 of four polymer samples with cylinder shape for ultrasonic pulse transmission measurement, (c) Group #2 of four polymer samples with cylinder shape for DARS measurement, and (d) Group #3 of four polymer samples with irregular shape for DARS measurement. Dimensions of the samples in the measurements can be found in Tables 4, 5, 6 and 8.

cavity. In essence, the second term on the right side of equation (8) can no longer be ignored in this case, so it is not proper to use equation (10) or (11) to estimate acoustic properties.

4. Laboratory Measurements

4.1. Validation of DARS Measurement

[22] In the DARS measurement, either a test sample or a calibration sample is measured along the longitudinal axis of the cavity at intervals of 6 mm. The scanning frequency at every measurement location ranges from 700 Hz to 1200 Hz. Figure 1 (top) shows a typical curve of the normalized pressure amplitude, with respect to the maximum amplitude, versus the scanning frequency at a measurement location. The resonant frequency at each measurement location can be obtained using the Lorentzian curve fitting method. In the current algorithm, only the resonant frequency measured at a particular measurement location (the velocity node) is used to estimate the compressibility of a sample. Also, we can obtain the resonant frequency f_0 by measuring the empty cavity, and finally, we can estimate the compressibility of a sample according to equation (12) or (13).

[23] In this work, we first apply the DARS and ultrasonic measurements to six standard Lucite samples with different dimensions, and then compare the measured results by the two independent laboratory techniques. Each Lucite sample is calibrated using a standard aluminum sample with the same dimensions. The six pairs of standard aluminum and Lucite samples are shown in Figure 11a. Results for both the ultrasonic and DARS measurements are listed in Table 3; the maximum relative error is about 6%. Considering that the acoustic wave propagating in the type of Lucite has almost no dispersion, the results indicate that the DARS technique provides an estimate of the compressibility comparable to the ultrasonic method.

[24] The three-dimensional DARS numerical simulation demonstrates the applicability of DARS to irregular samples. In this work, laboratory measurements were conducted to verify the numerical result that the perturbation in the DARS

Table 4. Ultrasonic Pulse Transmission Measurements of Four Synthetic Polymers

Measured Sample	Material	Diameter (mm)	Length (mm)	Mass (g)	Density (g/cm^3)	Vp (m/s)	Vs (m/s)	κ (GPa^{-1})
S-1-1	Nylon-1	52.32	49.74	121.96	1.14	2703.80	1123.02	0.155763
S-2-1	Ester	48.62	50.30	104.99	1.12	1819.49	/	0.268817
S-3-1	Nylon-2	30.40	50.24	34.96	0.96	2724.32	1329.82	0.206186
S-4-1	Rubber	30.71	50.32	60.44	1.62	1978.76	/	0.15748

Table 5. DARS Measurements of Four Polymer Samples With Cylinder Shape

Measured Sample	Diameter (mm)	Length (mm)	Density (g/cm^3)	f_{mear} (Hz)	κ (GPa^{-1})
S-1-2	29.97	50.00	1.140	718.04	0.1612
S-2-2	29.62	50.59	1.124	717.11	0.4122
S-3-2	30.60	50.16	0.959	717.25	0.2268
S-4-2	30.50	50.20	1.622	716.77	0.3144

measurement is only a function of the test sample volume and not the sample shape. Four types of polymer material (nylon-1, nylon-2, ester, and rubber) were obtained and machined into three sets, shown in Figures 11b–11d. Two sets have regular cylinder shapes and are used to perform ultrasonic and DARS measurements, respectively. Another set is irregularly shaped for the DARS measurements. The ultrasonic measurement results are listed in Table 4. Noticeably, no shear wave signal is received by a shear wave transducer for the two samples, ester(S-1-2) and rubber(S-1-4); thus, the shear moduli of these two samples are assumed to be extremely low or zero, which coincides with the description of the acoustic properties of rubber samples according to ultrasonic handbook [*Feng*, 1999]. The resultant compressibility for the first set of samples is listed in Table 4. Subsequently, we apply DARS measurements to the other two sets of samples shown in Figures 11c–11d, and obtain the compressibility listed in Tables 5 and 6. It should be noted that, for the third set of samples shown in Figure 11d, the volumes of the irregular samples are determined by dividing the mass by the density since these quantities can be accurately measured. Finally, the compressibility parameters obtained through ultrasonic and DARS measurements are listed in Table 7. An obvious conclusion is that DARS technique is capable of providing a comparable estimation of the compressibility between two samples of each material having regular and irregular shapes, respectively. The maximum relative error observable in our measurements is about 6%. The performance of the DARS measurement technique is relevant in cases when samples with regular shapes are not available. Also, we observe that for the nylon-1 and nylon-2 samples, the compressibility estimated by the ultrasonic and DARS measurements is comparable to each other; however, the two measurement techniques provide different results for the other two types of samples, ester and rubber. We attribute this observation to the different dispersion properties in the different types of samples.

4.2. Bulk Modulus Measurement of Small Irregular Rubber Samples

[25] To apply the DARS technique, we measure a variety of rubber samples. The bulk modulus is important to the understanding of the elastomer structure in polymer chain mechanics [*Burns et al.*, 1990]. Despite its importance, the bulk modulus has been the least studied of the elastic properties of elastomers, partly due to the practical difficulty in measuring it with high accuracy [*Burns et al.*, 1990; *Peter and Roland*, 2002; *Simonetti and Cawley*, 2005; *Guillot and Trivett*, 2003]. As discussed in previous sections, DARS has high accuracy for soft samples such as elastomers, and the technique is also applicable to small irregular samples within a relatively low frequency range. These advantages make DARS especially suitable for measuring the bulk modulus of elastomers.

[26] Different types of commercial rubber tubing were used for this test. There is no special sample preparation needed; the tubing is just cut into short pieces. To demonstrate the ability to measure an irregular sample, we also measured a rubber O-ring. Figure 12a shows the samples

Table 6. DARS Measurements of Four Polymer Samples With Irregular Shapes

Measured Sample	Volume (cm^3)	f_{mear} (Hz)	κ (GPa^{-1})
S-1-3	1.140	724.27	0.1576
S-2-3	1.124	720.52	0.3937
S-3-3	0.959	721.78	0.2419
S-4-3	1.622	722.08	0.2972

Table 7. Comparison of Compressibility Parameters Among Three Measurements for Four Types of Polymers[a]

Sample Material	κ (GPa^{-1})			Relative Error (%)
	Group #1	Group #2	Group #3	
Nylon-1	0.155763	0.1612	0.1576	2.2
Ester	0.268817	0.4122	0.3937	4.5
Nylon-2	0.206186	0.2268	0.2419	−6.7
Rubber	0.15748	0.3144	0.2972	5.5

[a]See Tables 4–6 and Figures 11b–11d. Ultrasonic measurement is applied to Group #1, and DARS measurements to Groups #2 (regular shape) and #3 (irregular shape). Relative error is between Groups #2 and #3.

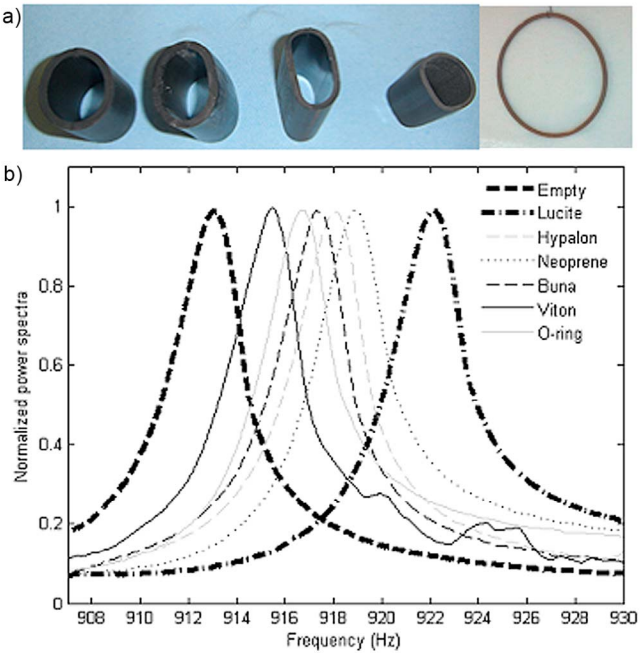

Figure 12. DARS measurements of several rubbery elastomers with irregular shapes. (a) Five rubbery elastomers with irregular shapes from left to right: Hypalon, Neoprene, Buna, Viton and O-ring. (b) Resonant frequency spectra acquired from DARS for the rubbery samples shown in Figure 12a. These are the data used to estimate the bulk moduli of the rubber samples tested.

Table 8. Ultrasonic Pulse Transmission and DARS Measurements of Six Standard Lucite Samples With Different Dimensions[a]

Measured Sample	Diameter (mm)	Length (mm)	Calibration Sample	Ultrasound κ (GPa^{-1})	DARS κ (GPa^{-1})	Relative Error (%)
lu_25_30	24.697	30.050	al_25_30	0.1763	0.1784	1.19
lu_25_25.6	24.960	25.598	al_25_25.6	0.1759	0.1731	−1.59
lu_25_60	25.821	59.780	al_25_60	0.1764	0.1675	−5.04
lu_15_71.1	14.821	70.963	al_15_71.1	0.1768	0.1870	5.76
lu_25_50	25.818	49.718	al_25_50	0.1755	0.1866	6.32
lu_20_40	20.048	40.003	al_20_40	0.1753	0.1860	6.10

[a]Six standard aluminum samples with the same dimension are used as calibration samples. (See Figure 11a.)

used in this test. A beaker with a precision of 0.2 cm^3 is used to measure the sample volume.

[27] The cavity in this experiment has a length of 46 cm, which is longer than the one used in the previous experiments. The resonant frequency for the empty cavity is f_0 = 912.92 Hz. Lucite is used as a standard sample for the calibration, and its parameters are listed in Table 8. The resonant frequency changes from f_0 to f_1 due to the Lucite sample being loaded at the center of the cavity. Figure 12b displays the DARS data collected in this experiment.

[28] As indicated by the simulation study in Section III, the DARS perturbation equation provides higher accuracy for soft samples such as elastomers. Therefore, in this experiment we can simply use equation (12) with $b = 1$ for the bulk modulus estimation. For this case, only one standard sample is needed for the calibration. The estimated bulk moduli for the test samples are shown in Table 9. In this table, the bulk modulus K is calculated from the resonant frequency f_1 using the perturbation equation. The sound speed c is calculated from $c = (\kappa/\rho)^{1/2}$, assuming that the shear wave velocity of the elastomers is zero. The DARS-based laboratory measurement technique is capable of obtaining the bulk modulus estimation for such elastomers, with results comparable to the experimental results reported in the literature [*Burns et al.*, 1990; *Peter and Roland*, 2002; *Simonetti and Cawley*, 2005; *Guillot and Trivett*, 2003].

5. Concluding Remarks

[29] A prototype of the DARS system, operating in the frequency range of one kilohertz, is developed to extract the acoustic properties of samples. This novel laboratory measurement technique is based on changes in the resonant frequencies of a cavity perturbed by the introduction of a small test sample. The cavity's first mode resonant frequency can be used to determine the acoustic properties of the samples. Compared with the stress-strain approach (another important low-frequency measurement technique), the DARS-based measurement is less time-consuming and easier to implement, since the DARS measurement concept is based on perturbation theory. The numerical simulation and experimental results indicate that DARS can be a useful technique with the amended DARS perturbation formula over a large compressibility range. In summary, DARS is capable of obtaining the acoustic properties of samples under the following conditions: (1) very low frequencies ~1000 Hz; (2) broad measurement bandwidth ~10,000 Hz; (3) narrow band measurement at a center frequency around 1000 Hz; (4) acoustically small samples, also implying low frequencies; and (5) samples with irregular shapes.

[30] Despite these advantages, there are some limitations to the current DARS system. First, the DARS system is not capable of handling high pressure and high temperature. Subsequently, DARS loses some ability to simulate in situ conditions, mostly for measurements on rock samples. Second, DARS is currently an open system; thus, the property of the cavity fluid (silicone oil) is more or less affected by changes in the ambient temperature as well as any introduction of air bubbles during the measurements. As a result, the resonant frequencies either with or without a sample are subject to slight fluctuations. This is a principal error source in the acoustic properties estimation. Ideally, an airproof cavity and a constant temperature should be used when measuring the resonant frequencies. Further updates to the DARS prototype must address these important issues.

[31] Furthermore, our current knowledge indicates that the DARS system performs better with samples of low and medium compressibility than with samples of high compressibility, in terms of an accurate estimation of acoustic properties. A considerable amount of additional theoretical, numerical, and experimental research is needed to provide further insight into the DARS measurements.

Table 9. Results for the Rubber Samples[a]

Name	V (cm^3)	ρ (g/cm^3)	f_1 (Hz)	K (GPa)	c (m/s)
Hypalon	14.3	1.25	917.93	1.89	1228
Neoprene	14.0	1.36	918.82	2.44	1337
Buna	11.1	1.27	917.26	2.17	1302
Viton	6.1	1.75	915.32	2.19	1118
O-ring	10.6	1.74	916.61	1.87	1039

[a]Resonance frequency for the empty cavity is 912.92 Hz, and a standard Lucite sample is for calibration in equation (12).

[32] **Acknowledgments.** This work is sponsored by Program 973, the Fundamental Study on the Geophysical Prospecting of the Heterogenuos Oil and Gas Reservoirs (grant 2007CB209600), Program for Changjiang Scholars and Innovative Research Team in University (PCSIRT), Nation Natural Science Foundation of China Research (grant 40704024), Science Foundation of China University of Petroleum, Beijing (KYJJ2012–05-02), and the Specialized Research Fund for the Doctoral Program of Higher Education (grant 20070425029). The authors also would like to thank Jianxin Wei of China University of Petroleum-Beijing for his help in conducting ultrasonic measurements, and Hongsheng Zhou of Shanghai Acoustics Laboratory, Chinese Academy of Sciences, for helping us design the piezoceramic source in the DARS measurements.

References

Adams, R. D., and J. Coppendale (1976), Measurement of the elastic moduli of structural adhesives by a resonant bar technique, *J. Mech. Eng. Sci.*, *18*(3), 149–158, doi:10.1243/JMES_JOUR_1976_018_025_02.

Batzle, M. L., D.-H. Han, and R. Hofmann (2006), Fluid mobility and frequency-dependent seismic velocity—Direct measurements, *Geophysics*, *71*, N1–N9, doi:10.1190/1.2159053.

Birch, F. (1960), The velocity of compressional waves in rocks to 10 kilobars, part 1, *J. Geophys. Res.*, *65*(4), 1083–1102, doi:10.1029/JZ065i004p01083.

Birch, F. (1961), The velocity of compressional waves in rocks to 10 kilobars, part 2, *J. Geophys. Res.*, *66*(7), 2199–2224, doi:10.1029/JZ066i007p02199.

Bulau, J. R., S. R. Tittmann, and M. Abdel-Gawad (1983), Attenuation and modulus dispersion in fluid saturated sandstone, *Eos Trans. AGU*, *64*, 323–324.

Burns, J., P. S. Dubbelday, and R. Y. Ting (1990), Dynamic bulk modulus of various elastomers, *J. Polym. Sci., B, Polym. Phys.*, *28*, 1187–1205, doi:10.1002/polb.1990.090280715.

Cadoret, T., D. Marion, and B. Zinszner (1995), Influence of frequency and fluid distribution on elastic wave velocities in partially saturated limestones, *J. Geophys. Res.*, *100*, 9789–9803, doi:10.1029/95JB00757.

Chen, L., C. K. Ong, and B. T. G. Tan (1999), Amendment of cavity perturbation method for permittivity measurement of extremely low-loss dielectrics, *IEEE Trans. Instrum. Meas.*, *48*(6), 1031–1037, doi:10.1109/19.816109.

Clark, V. A. (1980), Effects of volatiles on seismic attenuation and velocity in sedimentary rocks, PhD dissertation, Tex. A&M Univ., College Station.

Demarest, H., Jr. (1971), Cube-resonance method to determine the elastic constants of solids, *J. Acoust. Soc. Am.*, *49*, 768–775, doi:10.1121/1.1912415.

Feng, R. (1999), Ultrasonic engineering material, in *Ultrasonic Handbook*, chap. 2, pp. 134–138, Nanjing Univ. Press, Nanjing, China.

Gribb, T., and R. Cooper (1998), A high-temperature torsion apparatus for the high-resolution characterization of internal friction and creep in refractory metals and ceramics: Application to the seismic-frequency, dynamic response of Earth's upper mantle, *Rev. Sci. Instrum.*, *69*(2), 559–564, doi:10.1063/1.1148694.

Harris, J. M., Y. L. Quan, and C. T. Xu (2005), Differential acoustic resonance spectroscopy: An experimental method for estimating acoustic attenuation in porous media, *SEG Expanded Abstr.*, *24*, 1569–1572, doi:10.1190/1.2147992.

Guillot, F. M., and D. H. Trivett (2003), A dynamic Young's modulus measurement system for highly compliant polymers, *J. Acoust. Soc. Am.*, *114*(3), 1334–1345, doi:10.1121/1.1604121.

Jackson, I., H. Schijns, D. R. Schmitt, J. Mu, and A. Delmenico (2011), A versatile facility for laboratory studies of viscoelastic and poroelasctic rock, *Rev. Sci. Instrum.*, *82*, 064501, doi:10.1063/1.3592154.

Lucet, N., P. N. J. Rasolofosaon, and B. Zinszner (1991), Sonic properties of rocks under confining pressure using the resonant bar technique, *J. Acoust. Soc. Am.*, *89*(3), 980–990, doi:10.1121/1.400643.

Mehl, J. B. (1978), Analysis of resonance standing-wave measurements, *J. Acoust. Soc. Am.*, *64*(5), 1523–1525, doi:10.1121/1.382096.

Migliori, A., and J. L. Sarrao (1997), *Resonant Ultrasound Spectroscopy: Applications to Physics, Materials Measurements, and Non-destructive Evaluation*, John Wiley, New York.

Murphy, W. F. (1982), Effects of microstructure and pore fluids on the acoustic properties of granular sedimentary materials, PhD dissertation, Dep. of Geophys., Stanford Univ., Palo Alto, Calif.

Peter, H. M., and C. M. Roland (2002), Acoustic and dynamic mechanical properties of a polyurethane rubber, *J. Acoust. Soc. Am.*, *111*(4), 1334–1345, doi:10.1121/1.1459465.

Simonetti, F., and P. Cawley (2005), On the measurement of the Young's modulus of small samples by acoustic interferometry, *J. Acoust. Soc. Am.*, *118*(2), 832–840, doi:10.1121/1.1942387.

Spencer, J. W. (1981), Stress relaxation at low frequencies in fluid saturated rocks: Attenuation and modulus dispersion, *J. Geophys. Res.*, *86*, 1803–1812, doi:10.1029/JB086iB03p01803.

Sucher, M., and J. Fox (1963), *Handbook of Microwave Measurements*, 3rd ed., Polytechnic, Brooklyn, N. Y.

Tittmann, B. R., V. A. Clark, J. M. Richardson, and T. W. Spencer (1980), Possible mechanisms for seismic attenuation in rocks containing small amounts of volatiles, *J. Geophys. Res.*, *85*, 5199–5208, doi:10.1029/JB085iB10p05199.

Ulrich, T. J., K. R. McCall, and R. A. Guyer (2002), Determination of elastic moduli of rock samples using resonant ultrasound spectroscopy, *J. Acoust. Soc. Am.*, *111*, 1667–1674, doi:10.1121/1.1463447.

Winkler, K. (1979), The effects of pore fluids and frictional sliding on seismic attenuation, PhD dissertation, Dep. of Geophys., Stanford Univ., Palo Alto, Calif.

Winkler, K. W., A. Nur, and M. Gladwin (1979), Frictional sliding and seismic attenuation in rocks, *Nature*, *277*, 528–531, doi:10.1038/277528a0.

Wyllie, M., A. Gregory, and G. Gardner (1956), Elastic wave velocities in heterogeneous and porous media, *Geophysics*, *21*, 41–70, doi:10.1190/1.1438217.

Xu, C. T. (2007), Estimation of effective compressibility and permeability of porous materials with Differential Acoustic Resonance Spectroscopy," PhD dissertation, Dep. of Geophys., Stanford Univ., Palo Alto, Calif.

Xu, C. T., J. M. Harris, and Y. L. Quan (2006), Estimating flow properties of porous media with a model for dynamic diffusion, *SEG Expanded Abstr.*, *25*, 1831–1835, doi:10.1190/1.2369880.

Yin, C. S., M. L. Batzle, and B. J. Smith (1992), Effects of partial liquid/gas saturation on extensional wave attenuation in Berea Sandstone, *Geophys. Res. Lett.*, *19*, 1399–1402, doi:10.1029/92GL01159.

Zadler, B. J., J. H. L. Le Rousseau, J. A. Scales, and M. L. Smith (2004), Resonant ultrasound spectroscopy: Theory and application, *Geophys. J. Int.*, *156*, 154–169, doi:10.1111/j.1365-246X.2004.02093.x.